# Gyrokinetic Modeling of Linear Tearing Mode

T. Jitsuk, A. Di Siena, Z. R. Williams, M. J. Pueschel, and P. W. Terry

**University of Wisconsin-Madison**
**Center for Plasma Theory and Computation**
**Report UW-CPTC 22-3**

May 27, 2022



Support for this research came from the U.S. Department of Energy, Office of Science Award Number DE-FG02-85ER53212.

# Gyrokinetic Modeling of Linear Tearing Mode

**T. Jitsuk[1,*], A. Di Siena[2], Z.R. Williams[3], M.J. Pueschel[4], and P.W. Terry[1]**

[1] *Department of Physics, University of Wisconsin-Madison, WI 53706, USA*
[2] *Max-Planck-Institut für Plasmaphysik, D-85748 Garching, Germany*
[3] *Department of Physics, Hope College, Holland, MI 49423 USA*
[4] *Dutch Institute for Fundamental Energy Research, 5612 AJ Eindhoven, The Netherlands*

[*] *jitsuk@wisc.edu*

**Abstract:**
Macro-scale tearing modes are excited during plasma operations on the Madison Symmetric Torus, a reversed-field pinch (RFP). These fluctuations have significant impacts on micro-scale instabilities and turbulent transport even in improved-confinement regimes. This observation motivates the need for modeling of the interplay of fluctuations at different scales using the gyrokinetic code GENE. Previous work modeled tearing-mode activity by implementing current-gradient drive as part of the fluctuating distribution function, coupled nonlinearly with turbulence fluctuations and zonal flows. To be able to more realistically model tearing modes, a shifted-Maxwellian distribution has been implemented in GENE for global simulations, consistent with the experimental $q-$profile. The implementation has been benchmarked against linear flux-tube simulations through scans over plasma parameters. Additionally, comparisons are shown with global tearing results from other gyrokinetic and fluid codes. The work described herein lays the foundation for nonlinear simulation and analysis of the interaction of tearing modes and gyroradius-scale instabilities in the RFP.


## 1. Introduction

Global tearing mode activity is a fundamental aspect of plasma dynamics in the reversed-field pinch (RFP), and has been widely studied. Tearing modes grow to finite amplitude from a current-gradient-driven instability, and then in the nonlinear state can couple among themselves or couple with small-scale fluctuations, leading to different consequences. For example, detailed analyses of experimental measurements and nonlinear MHD computation have demonstrated that coupling between tearing modes of different poloidal mode number $m$ results in conversion of poloidal magnetic flux in the core region to toroidal magnetic flux near the reversal surface, producing self-generated toroidal flux (dynamo effect) [10, 11]. Interactions of multiple tearing modes resonant at different radii also enhance energy and momentum transport [8, 9]. Suppression of tearing modes by current profile control in pulsed poloidal current drive (PPCD) experiments has produced improvements in plasma confinement, with increases in plasma beta and temperature, and reduction of the electron heat diffusivity [2]. Fluctuation interactions involving tearing modes occur not only in global scales but also happen across an extended range of scales. Tearing modes are known to produce a cascade to small scales, where interactions can continue to involve MHD fluctuations, or include micro-scale instabilities and turbulence. An example of a multiscale interaction effect was demonstrated in gyrokinetic simulation of

$\nabla n$-TEM turbulence in the RFP with a representation of tearing mode activity in terms of an external magnetic field perturbation. The simulations showed that the magnetic fluctuations suppressed the zonal flows generated nonlinearly in TEM turbulence, resulting in an increase of the electromagnetic heat flux [21].

Unlike the physics of self-interacting tearing modes, which has been extensively studied, interactions of micro- and macro-scale fluctuations have received limited attention and consequently are not as well-understood. Given their potential for significantly influencing RFP dynamics and confinement, multiscale interactions are an important topic for future study. The limited progress on multiscale interactions to date is due, at least in part, to the fact that coupling of two distinct scales is difficult to treat computationally. While studies of single-scale tearing modes and nonlinear couplings of different helicities can be done solely within MHD models, coupling with micro instabilities needs models that are well suited for gyro-scale drift-wave physics. One class of drift-wave-capable models is gyrokinetics, which generally provides the most comprehensive representation of microscale instability physics. Although many types of micro-instability have been studied and their representation is well-established in the gyrokinetic framework, work on computation with global scale MHD modes has been limited. Given an interest in studying multi-scale physics, MHD modes such as tearing modes need to be correctly modeled in the gyrokinetic approach. This can be computationally challenging if fidelity to experiment requires realistic representation of the confining geometry.

A previous study of multi-scale interactions in RFP plasmas using the gyrokinetic code GENE imposed a constant-in-time external $A_{\parallel}$ as a crude model for tearing-mode activity [1, 21]. However, MHD-scale tearing instabilities in experiment are driven by a background current gradient parallel to the mean magnetic field. Therefore to better model this situation a self-consistent calculation is needed. To this end a subsequent modeling effort implemented a current-gradient drive as part of the fluctuating distribution function. The implementation allowed for a sinusoidal current profile with adjustable magnitude and phase. The implementation was done in a local slab geometry. Several aspects of this improved but still approximate modeling approach proved to be problematic. The computation was limited to local simulations, which do not allow for a realistic equilibrium. For example, geometrical effects such as magnetic curvature drifts were not included in the model. Most critically, linear solutions of the gyrokinetic model equations resulted in slab-specific intermediate-scale modes. As these are not present in experiment, they interfere with the study of experimentally relevant multi-scale interactions.

To more realistically model tearing modes, a shifted-Maxwellian has been implemented for the equilibrium distribution in GENE for use in global simulations, consistent with a specified safety factor profile. Detailed calculations related to the implementation of the shifted Maxwellian distribution are presented in this report, including the equilibrium distribution with shifted velocity, its effect on the perturbed distribution and the instability driving terms, and its modification of velocity moments that enter into the calculation of the self-consistent fields. The implementation has been benchmarked against linear flux-tube simulations through scans over plasma parameters. Comparisons are also shown with global tearing results from a reduced fluid model and gyrokinetic codes. Linear tearing modes in the RFP under its equilibrium profiles for a non-reversed discharge with pulsed poloidal current drive are obtained in a full three dimensional computation. The linear eigenmodes are analyzed compared with theoretical and experimental results. These linear modes will provide the basis for studying multi-scale interactions with gyroradius-scale instabilities in future work.

The remainder of this report is organized as follows. Details of numerical approach and its implementation are discussed in Section 2. Numerical benchmarking efforts against a variety of published results are elaborated in Section 3. A summary and discussion are provided in Section 4.

## 2. Numerical Approach

### 2.1. *Global Gyrokinetic Code* GENE

The gyrokinetic framework provides a favorable computational scheme for nonlinear coupling between fluctuations in a range of scales. Here, we use the global version of GENE code, which allows implementation of a non-Maxwellian distribution [5, 6]. GENE solves a Vlasov-Maxwell system of equations based on a $\delta f$ approach, i.e., the total distribution $f$ is split into the static background distribution $F_0$ and the small perturbed distribution $\delta f$, such that $f = F_0 + \delta f$. Writing $f$ in terms of modified distribution $g$ given below, the simplified form of the gyrokinetic equation for each plasma species is represented by

$$\frac{\partial}{\partial t} g_j = \mathscr{L}_j[g_j] + \mathscr{N}[g_j, g_j']. \tag{1}$$

In this equation, $g_j$ is the modified distribution function of species $j$, which is related to the distribution function $f_j$ as $g_j = f_j - q_j/(cm_j)\partial_{v_\parallel} F_{0j}\bar{A}_\parallel$. $\mathscr{L}$ is the linear operator containing the instability driving gradients for both small-scale drift-wave instabilities and large-scale current-driven modes. It also contains background equilibrium distribution which will be elaborated more in the next section. $\mathscr{N}$ is the $\mathbf{E}\times\mathbf{B}$ nonlinearity that couples different interacting modes. In this report, the main focus is on linear solutions and the nonlinearity is set to zero; however, it will be included in later work when nonlinear interactions are considered. GENE solves this gyrokinetic equation self-consistently with coupled field equations. Instabilities are characterized by growth of fluctuating fields, i.e., $\tilde{A}_\parallel$ and $\tilde{\phi}$.

### 2.2. *Shifted Maxwellian Implementation*

The instabilities that are driven by the current gradient $J_\parallel$ (tearing modes in this work), the shifted Maxwellian background distribution, and the shifted velocity must all reflect the realistic driving mechanism. The original GENE code utilizes a Maxwellian distribution for the unperturbed background distribution, which results in zero parallel current density under the first moment of the parallel velocity. Hence, the shifted Maxwellian (SM) distribution function is implemented in the background and as a part of the linear operator to reflect the phenomena observed in the RFP. This distribution replaces the Maxwellian distribution. The background distribution $F_{\mathrm{SM}}$ of each particle species $j$ has the form

$$F_{\mathrm{SM},j} = \frac{n_{0j}(x)\, m_j^{3/2}}{(2\pi T_{0j}(x))^{3/2}} \exp\left(-\frac{(m_j/2)(v_\parallel - v_{\parallel 0,j}(x))^2 + \mu B_0}{T_{0j}(x)}\right). \tag{2}$$

For each plasma species $j$, $F_{\mathrm{SM},j}$ contains parts of equilibrium pressure profile, the density $n_{0j}(x)$, and temperature $T_{0j}(x)$, respectively. $m_j$ is the particle mass, $B_0$ is the equilibrium magnetic field, and $v_{\parallel 0j}$ is the shifted velocity in the parallel direction. This shifted velocity is normalized with respect to the thermal velocity of each plasma species $v_{\mathrm{Th},j} = \sqrt{2\hat{T}_{0j}(x_0)/m_j}$ at the reference position in the simulation domain. Various functions and terms involving the Vlasov-Maxwell equations under the shifted Maxwellian distribution need to be considered and calculated before implementing them into GENE. The first important term is the radial derivative of the background distribution contributing to

electromagnetic driving terms in the Vlasov equation.

$$\begin{aligned}\nabla_x \hat{F}_{\mathrm{SM},\,j} &= \left[\frac{\nabla_x \hat{n}_{0j}}{\hat{n}_{0j}} - \frac{3}{2}\frac{\nabla_x \hat{T}_{0j}}{\hat{T}_{0j}} - \nabla_x\left(\frac{(\hat{v}_{\|0,j}-\hat{v}_{0j})^2+\hat{\mu}B_0}{\hat{T}_{0j}}\right)\right]\hat{F}_{\mathrm{SM},\,j},\\ &= \left[\nabla_x \ln \hat{n}_{0j} + \nabla_x \ln \hat{T}_{0j}\left(\frac{(\hat{v}_{\|}-\hat{v}_{\|0,j})^2+\hat{\mu}B_0}{\hat{T}_{0j}} - \frac{3}{2}\right)\right.\\ &\quad \left. + \frac{2(\hat{v}_{\|}-\hat{v}_{0j})\nabla_x \hat{v}_{0j} - \hat{\mu}\nabla_x B_0}{\hat{T}_{0j}}\right]\hat{F}_{\mathrm{SM},\,j}.\end{aligned}$$

The term $\hat{\mu}\nabla_x B_0/\hat{T}$ generally cancels with $\mu B_0 \partial_{v_\|} F_0/(m v_\|)$ in the linear operator if the distribution is symmetric along the parallel velocity direction, i.e., in the terms

$$(\mathbf{v}_{\mathrm{D}} + \mathbf{v}_{\nabla B} + \mathbf{v}_{\mathrm{c}})\cdot\left(\nabla F_0 - \frac{\mu \nabla B_0}{m v_\|}\frac{\partial F_0}{\partial v_\|}\right). \tag{3}$$

However, for the SM distribution, these terms do not completely cancel but combined to $(\hat{v}_{\|0,j}/\hat{v}_\|)\hat{\mu}_0\partial_x B_0$, which is also implemented as part of the drive term. We define $\omega_{nj} \equiv -L_{\mathrm{ref}}\nabla_x \ln \hat{n}_{0j}$ and $\omega_{Tj} \equiv -L_{\mathrm{ref}}\nabla_x \ln \hat{T}_{0j}$ as the density and temperature gradient scaled lengths, respectively. The simplified drive terms read,

$$\begin{aligned}\nabla_x \hat{F}_{\mathrm{SM},\,j} = &-\frac{\hat{F}_{\mathrm{SM},\,j}}{L_{\mathrm{ref}}} \times \left[\omega_{nj} + \omega_{Tj}\left(\frac{(\hat{v}_{\|}-\hat{v}_{\|0,j})^2+\hat{\mu}B_0}{\hat{T}_{0j}} - \frac{3}{2}\right)\right.\\ &\left. - \frac{2(\hat{v}_{\|}-\hat{v}_{\|0,j})L_{\mathrm{ref}}\nabla_x \hat{v}_{\|0,j} - (\hat{v}_{\|0,j}/\hat{v}_{\|})\hat{\mu}L_{\mathrm{ref}}\nabla_x B_0}{\hat{T}_{0j}}\right].\end{aligned} \tag{4}$$

The first two terms $\omega_{nj}$ and $\omega_{Tj}$ on the right-hand side of the equation are responsible for the well-known electrostatic drives associated with micro-instabilities. The last term involving the gradient of the shifted velocity introduces the new driving force into the system, i.e., the current gradient drive as $\nabla v_{\|0} \sim \nabla J_{\|0}$. There is also a residue of the SM distribution function. The appropriate background current density gradient responsible for the tearing mode drive is now obtained. Other velocity moments related to observable quantities such as electromagnetic heat and particle fluxes are also derived and implemented into the code.

### *2.3. Field Equations*

The plasma dynamics governed by the Vlasov equation are coupled with the field equations and calculated self-consistently. The linear tearing mode in this study is global; hence, the field equations contain the gyro-average in space with variations in the radial direction. The evolution of the perturbed electrostatic field component $\phi$ can be evaluated using the Poisson equation,

$$\nabla_\perp^2 \phi_1(\mathbf{x}) = -4\pi\sum_s q_s n_{1,s}(\mathbf{x}) = -4\pi\sum_s q_s M_{00,s}(\mathbf{x}). \tag{5}$$

Here, the density $n_{1,s}$ is written in terms of the zero-order moment of velocity, $M_{0,0,s}(\mathbf{x})$. Using the form of moments derived in the thesis of A. Di Siena [4], and neglecting the fluctuation of parallel magnetic field, one can write the electrostatic potential as

$$\nabla_\perp^2 \phi_1(\mathbf{x}) = -\frac{8\pi^2 q B_0}{m}\int\int\left\{\langle f_1(\mathbf{x}-\mathbf{r})\rangle\right. \tag{6}$$

$$+\left(\frac{\Omega}{B_0}\frac{\partial F_{\mathrm{SM}}}{\partial v_\|} - \frac{q}{cB_0}v_\|\frac{\partial F_{\mathrm{SM}}}{\partial \mu}\right)\left(A_{1,\|}(\mathbf{x}) - \langle \bar{A}_{1,\|}(\mathbf{x}-\mathbf{r})\right) \tag{7}$$

$$\left.+\left[\frac{q}{B_0}\left(\phi_1(\mathbf{x}) - \langle\bar{\phi}_1(\mathbf{x}-\mathbf{r})\rangle\right)\right]\frac{\partial F_{\mathrm{SM}}}{\partial \mu}\right\}\mathrm{d}v_\|\mathrm{d}\mu. \tag{8}$$

The parallel vector potential under Coulomb Gauge in the absence of equilibrium electric fields is calculated from the Ampère's law,

$$\nabla_\perp{}^2 A_{1,\parallel}(\mathbf{x}) = -\frac{4\pi q}{c} M_{10,s}(\mathbf{x}). \tag{9}$$

In terms of velocity moments as stated in Ref. [4], neglecting the fluctuation of the parallel magnetic field which can be very small, the Amère's law can be written as

$$\nabla_\perp^2 A_{1,\parallel}(\mathbf{x}) = -\frac{8\pi^2 q}{mc}\int\int\Bigg\{\langle f_1(\mathbf{x}-\mathbf{r})\rangle \tag{10}$$

$$+\left(\Omega\frac{\partial F_{\rm SM}}{\partial v_\parallel} - \frac{qv_\parallel}{c}\frac{\partial F_{\rm SM}}{\partial \mu}\right)\left(A_{1,\parallel}(\mathbf{x}) - \langle \bar{A}_{1,\parallel}(\mathbf{x}-\mathbf{r})\right) \tag{11}$$

$$+q\left(\phi_1(\mathbf{x}) - \langle\bar{\phi}_1(\mathbf{x}-\mathbf{r})\rangle\right)\frac{\partial F_{\rm SM}}{\partial \mu}\Bigg\}{\rm d}v_\parallel{\rm d}\mu. \tag{12}$$

By substituting the shifted Maxwellian and corresponding shifted velocity, the coupled field equations can be written in form of matrices as

$$\begin{bmatrix} c_1 & c_2 \\ c_3 & c_4 \end{bmatrix}\begin{bmatrix}\phi_1 \\ A_\parallel\end{bmatrix} = \begin{bmatrix} N_{00} \\ N_{10}\end{bmatrix}. \tag{13}$$

Hence, solving these equations gives

$$\begin{bmatrix}\phi_1 \\ A_\parallel\end{bmatrix} = \frac{1}{c_1c_3 - c_2c_4}\begin{bmatrix} c_4 & -c_2 \\ -c_3 & c_1\end{bmatrix}\begin{bmatrix} N_{00} \\ N_{10}\end{bmatrix},$$

where

$$c_1 = -\nabla_\perp^2\lambda_{\rm De}^2 - \frac{n_0\pi q^2}{T_0}\int\int\left[\frac{\partial F_{\rm SM}}{\partial\mu}\hat{\mathbf{1}} - \mathscr{G}^\dagger\left(\frac{\partial F_{\rm SM}}{\partial\mu}\right)\mathscr{G}\right]{\rm d}v_\parallel{\rm d}\mu, \tag{14}$$

$$c_2 = \frac{2\pi q^2 n_0}{mv_{\rm Th}}\int\int\left[\left(v_\parallel\frac{\partial F_{\rm SM}}{\partial\mu} - \frac{B_0}{2}\frac{\partial F_{\rm SM}}{\partial v_\parallel}\right)\hat{\mathbf{1}} - \mathscr{G}^\dagger v_\parallel\left(\frac{\partial F_{\rm SM}}{\partial\mu}\right)\mathscr{G}\right]{\rm d}v_\parallel{\rm d}\mu, \tag{15}$$

$$c_3 = -\frac{q^2\pi\beta_{\rm ref}n_0}{mv_{\rm Th}}\int\int v_\parallel\left[\frac{\partial F_{\rm SM}}{\partial\mu}\hat{\mathbf{1}} - \mathscr{G}^\dagger\frac{\partial F_{\rm SM}}{\partial\mu}\mathscr{G}\right]{\rm d}v_\parallel{\rm d}\mu, \tag{16}$$

$$c_4 = -\nabla_\perp^2 - \frac{q^2\pi\beta_{\rm ref}n_0}{m}\int\int\left[\left(B_0\frac{v_\parallel}{2}\frac{\partial F_{\rm SM}}{\partial v_\parallel} - v_\parallel^2\frac{\partial F_{\rm SM}}{\partial\mu}\right)\hat{\mathbf{1}} - \mathscr{G}^\dagger\left(v_\parallel^2\frac{\partial F_{\rm SM}}{\partial\mu}\right)\mathscr{G}\right]{\rm d}v_\parallel{\rm d}\mu, \tag{17}$$

$$N_{00} = q\pi n_0 B_0\int\mathscr{G}(g_1(\mathbf{x})){\rm d}v_\parallel{\rm d}\mu, \text{ and} \tag{18}$$

$$N_{10} = qn_0\pi\beta_{\rm ref}\frac{B_0 v_{\rm th}}{2}\int v_\parallel\mathscr{G}(g_1(\mathbf{x})){\rm d}v_\parallel{\rm d}\mu. \tag{19}$$

The operation $\mathscr{G}^\dagger A(\mathbf{x}-\mathbf{r})\mathscr{G}$ is the double gyroaverage operator, sometimes written as $\langle\bar{A}(\mathbf{x}-\mathbf{r})\rangle$ in other publications. The diagonal elements of the gyro-average matrix are written as $\hat{\mathbf{1}}$, $T_0 = T(x_0)$ and $n_0 = n(x_0)$ are the temperature and density at the reference position $x_0$, $v_{\parallel 0}$ is the shifted velocity normalized by thermal velocity $v_{{\rm Th},s}$, and $g_1(\mathbf{x})$ is the modified distribution function involved in calculation of the Vlasov equation.

### *2.4. Shifted Parallel Velocity*

The shifted Maxwellian distribution function needs the shifted velocity input profile $v_{\parallel 0}(r)$ in the direction parallel to the magnetic-field, which can be directly formulated from the equilibrium parallel

current density obtained from experiment as

$$J_{\parallel 0} = \sum_j n_{0j} q_j v_{\parallel 0,j} = \sum_j q_j \int v_{\parallel,j} F_{\mathrm{SM},j} \mathrm{d}^3\mathbf{v}. \tag{20}$$

Generally, the plasma of interest consists of two species, i.e., ions and electrons flowing in opposite directions. The current is written as

$$J_{\parallel 0,i} + J_{\parallel 0,e} = n_{\mathrm{e}0} e \hat{v}_{\parallel 0} v_{\mathrm{The}} \left(1 + \sqrt{(T_\mathrm{e}/T_\mathrm{i})(m_\mathrm{i}/m_\mathrm{e})}\right), \tag{21}$$

$$\therefore\ \hat{v}_{\parallel 0} = \frac{J_{\parallel 0}}{n_{\mathrm{e}0} e v_{\mathrm{The}}} \left(1 + \sqrt{(T_\mathrm{e}/T_\mathrm{i})(m_\mathrm{i}/m_\mathrm{e})}\right)^{-1}. \tag{22}$$

The current can also be extracted from the equilibrium profile of the safety factor, as the $q$-profile contains information about the toroidal and poloidal magnetic fields. For a large aspect-ratio circular cross-section, the $q-$profile can be approximated as

$$q(r) \simeq \frac{r}{R_0} \frac{B_\phi(r)}{B_\theta(r)}, \tag{23}$$

where $B_\phi(r)$ and $B_\theta(r)$ are toroidal and poloidal magnetic profiles, respectively. From Ampère's law $\mu_0 \mathbf{J} = \nabla \times \mathbf{B}$ in cylindrical approximation with $B_\theta \ll B_\phi \sim B_0$, the parallel current density therefore can be written as

$$J_{\parallel 0}(r) \approx \frac{1}{\mu_0} \left(\frac{1}{r} \frac{\partial (r B_\theta)}{\partial r}\right) = \frac{B_0}{R_0 \mu_0} \frac{\partial}{r \partial r} \left(\frac{r^2}{q(r)}\right). \tag{24}$$

The prefactor $B_0/(R_0\mu_0)$ is equivalent to the current density at the axis $J_{\parallel 0}$. Equating this expression to Eq. (22), the shifted velocity can be obtained as

$$\hat{v}_{\parallel 0} = \frac{J_{\parallel 0}}{n_{\mathrm{e}0} e v_{\mathrm{The}}} \left(1 + \sqrt{(T_\mathrm{e}/T_\mathrm{i})/(m_\mathrm{i}/m_\mathrm{e})}\right)^{-1} \left[\frac{\partial}{r \partial r} \left(\frac{r^2}{q}\right)\right], \tag{25}$$

or in terms of GENE parameters, the shifted velocity is equivalently written as

$$\hat{v}_{\parallel 0} = \frac{\sqrt{2} \varepsilon_a \rho_\mathrm{i}^*}{\beta_\mathrm{e}} \left(1 + \sqrt{(T_\mathrm{e}/T_\mathrm{i})/(m_\mathrm{i}/m_\mathrm{e})}\right)^{-1} \left[\frac{\partial}{r \partial r} \left(\frac{r^2}{q}\right)\right], \tag{26}$$

with $\beta_\mathrm{e} = 8\pi n_\mathrm{e} T_\mathrm{e}/B_0$, $\rho_\mathrm{i}^* = \rho_\mathrm{i}/a$, and $\varepsilon_a = a/R_0$.

## 3. Computational Benchmarking

The implementation of a shifted Maxwellian along with shifted velocity in the Vlasov-Maxwellian system of equations represents a significant modification to GENE, enabling global simulation of current-driven instability. It is important to test this implementation against different computational approaches, including work that is already published, to assure correct implementation.

### *3.1. Comparison with Results from Local Flux-Tube Simulation*

We start with comparisons to local simulations of a 2D slab magnetic geometry. GENE has previously been used to successfully model micro-instabilities in local flux-tube slab simulations [1,19,21]. Modeling of large-scale tearing mode was done by imposing a constant-in-time $A_\parallel^{\mathrm{ext}}$ into the perturbed distribution function and as a part of the linear operator. This external field is assigned through the value of the local shifted velocity. By now having a shifted Maxwellian distribution function in the linear drive term, the original GENE linear operator is modified [20] to enable tearing-mode modeling. An

additional difference between the local and global implementations is that while the local implementation has a limited ability to work only on the 2D slab geometry, the global implementation is extended to work in toroidal geometry such that the curvature terms are included. Since global implementation can be simplified to work in a 2D-slab geometry, it is tested against the local implementation which was used to produce tearing modes in [20].

Note that there is no actual $q$-profile associated with the computation in the local simulation; the magnitude of $v_{\|0}$ is determined by the expected $J_{\|0}$, which is represented by $A_{\|0}^{\rm ext}$. This velocity is also used as an input in the shifted Maxwellian for global simulation,

$$J_{\|0}^{\rm ext} = \frac{c}{4\pi}\frac{\partial B_{y0}}{\partial x} = \frac{c}{4\pi}\frac{\partial^2 A_{\|0}^{\rm ext}}{\partial x^2},$$
$$\therefore\ \hat{v}_{\|0} = \frac{c}{4\pi n_{0i} q_i v_{{\rm Th},i}}\left(1+\sqrt{(T_{\rm e}/T_{\rm i})(m_{\rm i}/m_{\rm e})}\right)^{-1}\frac{\partial^2 A_{\|0}^{\rm ext}}{\partial x^2}.$$

Writing the prefactors in terms of plasma parameters $\rho_{\rm i}^* = (c_i/\Omega_i)/L_{\rm ref}$, $\beta_{\rm e} = 8\pi n_{0iT_e}/B_0^2$, and using $\partial_x \sim k_{x,{\rm cs}}$, we obtain,

$$\hat{v}_{\|0} = \frac{k_{x,{\rm cs}}^2 \rho_{\rm i}^*}{\beta_{\rm e}/\sqrt{2}}\left(1+\sqrt{(T_{\rm e}/T_{\rm i})(m_{\rm i}/m_{\rm e})}\right)^{-1}\hat{A}_{\|0}^{\rm ext}. \tag{27}$$

The local simulation used a sinusoidal current profile. In terms of the shifted velocity it is written as $v_e(x) = -v_0\cos(k_{x{\rm cs}}x)$, as shown in Fig. 1. The simulation was performed in a simple slab magnetic geometry at $k_y = \rho^* = 1/(10\pi)$, $\beta_{\rm e} = 0.01$, $m_{\rm e}/m_{\rm i} = 1/1836$ and $J_{\|0} \sim v_{\rm shifted} = 1.0 v_{{\rm Th,j}}$. The local and global simulations both used the periodic boundary conditions in $x$ and $y$ directions. The mode structures are shown to be consistent with each other, as seen in Fig. 1. They exhibit even mode parity at the strongest gradient locations. The mode minima are at the flat current gradient locations. A scan over the driving gradient shows that the mode are destabilized and track each other, as shown in Fig. 2.

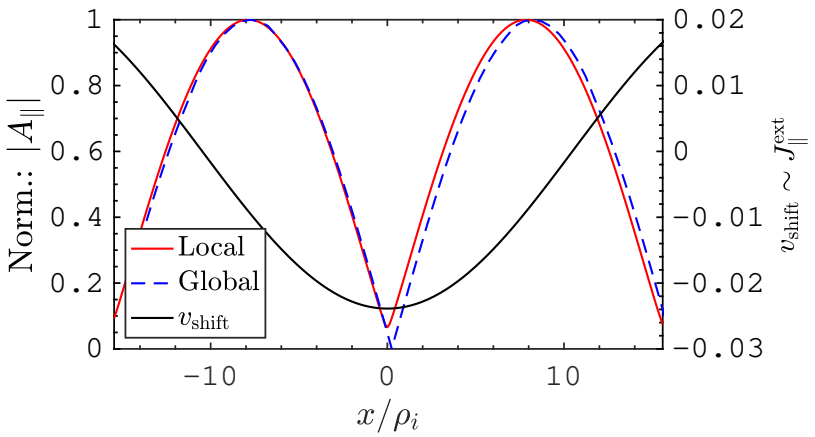


Fig. 1. Normalized radial mode structures of electrostatic potential of the tearing mode. Red solid-line is obtained from local simulation, Blue dashed-line is from global simulation. The simulations are perform by different implementations, but having the same set of parameters: ($m_{\rm e}/m_{\rm i} \sim 1/1836$ and plasma beta $\beta_{\rm e} = 0.1$, $\hat{v}_{\rm shift} \sim \hat{J}_{\|0} = 1.0$)

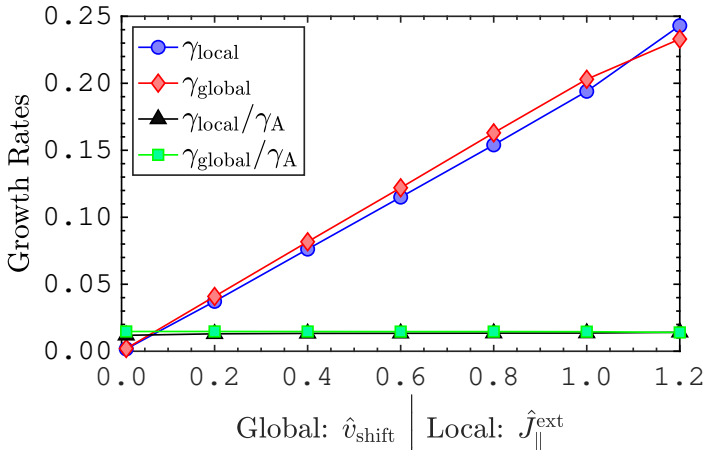


Fig. 2. Scan over shifted velocity, as the proxy for driving mechanism. The local simulation is set via $J_{\rm ext}$, while the global simulation is sets with $v_{\rm shift}$. ($m_{\rm e}/m_{\rm i} \sim 1/1836$ and plasma beta $\beta_{\rm e} = 0.1$)

The scans over mass and plasma beta are shown in Fig. 3, which shows that the two codes give consistent tearing mode growth rates. They track each other at low beta, i.e., the computations agree well in the electrostatic limit. When beta gets larger, the modes become more electromagnetic, and the results start to deviate from each other. It should be noted that the two simulations are not exactly the same implementation, as some differences can be found in the two approaches. The global simulation, however, is self-consistently calculated. When the growth rates are normalized by the Alfvén frequency, $\gamma_A = k_{x,cs}\partial_x B_{y0}^{\rm max}/\sqrt{4\pi m_i n_{\rm e0}} = k_{xcs}^2 A_{\parallel 0}^{\rm ext}\sqrt{2/\beta}$, the scans show the beta scaling of $\gamma/\gamma_{\rm A} \sim 1/\sqrt{\beta_{\rm e}}$ which are consistent with theory predictions [7]. From the plot in Fig. 3, the global simulations show better scaling than that of the local computation.

### 3.2. *Comparison with Results of a Resistive MHD Model*

Local flux-tube simulations in slab geometry do not take the curvature drift into account, and they also cannot correctly model plasmas in a three-dimensional system. Moreover, according to [20], the lab simulation produces intermediate scale modes intrinsic to the slab system. We need to test 3D simulations and study the ability to model tearing modes dynamics. To that end we here confirm the ability to capture the tearing mode in a toroidal system by reproducing the tearing mode structure and spectrum with safety factor and pressure profiles used in Ishizawa *et al.* (2009) [15]. These profiles have been shown to produce a prominent low-order tearing mode for studying thermal transport in the presence of magnetic fluctuations [15], island formation, and rotation [14], using reduced MHD calculation. In Ref. [15] the safety factor is expressed as

$$q = q_0\left\{1 + r_a^{2p}[(q_a/q_0)^p - 1]\right\}^{1/p}, \tag{28}$$

where the safety factor at the magnetic axis is $q_0 = 1.7$, and its value at the minor radius is $q_a = 4.0$. The exponent $p$ is equal to 4.0. The profile is plotted in Fig. (4), with the corresponding shifted velocity calculated using Eq. (26). The $q$-profile has a tearing mode that is resonant at the $q = 2$ surface at $r/a = 0.65$. The density and temperature profiles are given by

$$n_{\rm eq} = 0.8 + 0.2\exp(-4r_a^2), \tag{29}$$

$$T_{\rm eq} = 0.8 - 0.2\tanh[(r_a - 0.7)/0.2]. \tag{30}$$

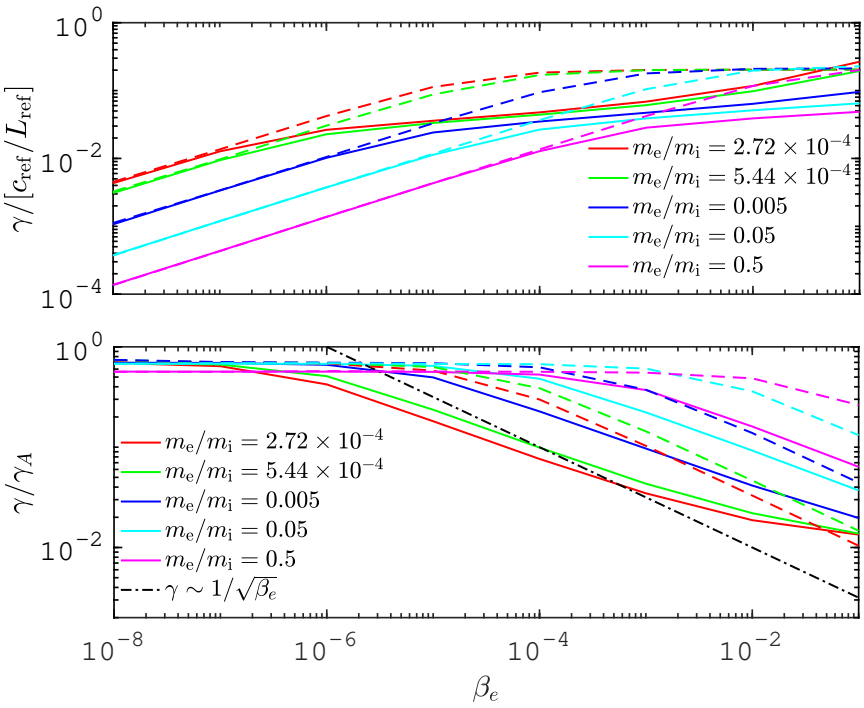


Fig. 3. Electron plasma beta $\beta_{\rm e}$ scan at different mass ratios with $v_{\rm shift} = 1$, $k_{x,\rm cs} = 0.2$. The solid lines are obtained from local simulations whereas the dashed lines are from global simulations. The back dashed-dotted line in the bottom panel is showing $\gamma/\gamma_A \sim 1/\sqrt{\beta_{\rm e}}$

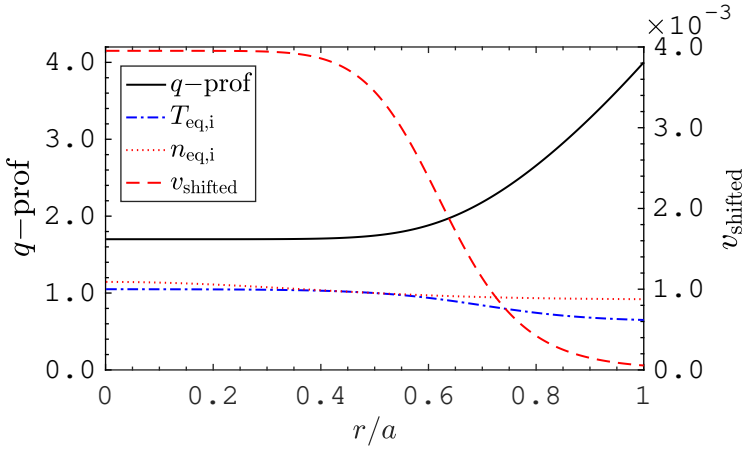


Fig. 4. Safety factor profile and corresponding shifted velocity. The pressure profiles are also included.

Simulations are performed with an aspect ratio of $R/a = 4$, the plasma beta in this case is $\beta_{\rm e} = 0.01$, and $\rho^* = \rho_{\rm i}/a = 1/80$. With these profiles, we show the tearing mode structure in Fig. (5), noting that it exhibits the characteristics of $m/n = 2/1$ mode structure. The radial mode structures of both $\phi$ and $A_\parallel$ are also characteristic of the tearing mode. To ensure that the new implementation reproduces tearing mode scalings, we perform a collisional scan to see how the mode responds to the collision frequency, which relates to the resistivity. The collisionality scan is displayed in Fig. 6, showing scaling results for the $n = 1$ tearing mode obtained from gyrokinetic simulation using Ishizawa's equilibrium profiles,

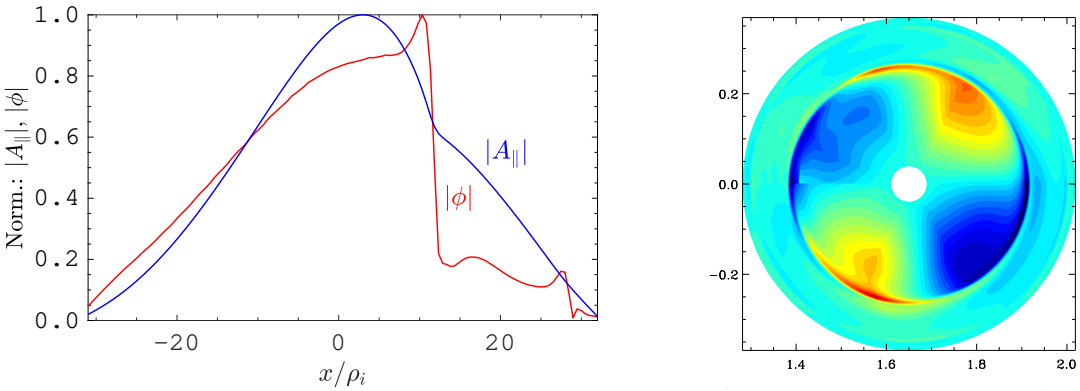


Fig. 5. Left: Radial mode structure of the tearing mode with $n = 1$ of Ishizawa's profile. The structure shows tearing mode charateristic of $m = 1$ and $m = 2$ at $r \approx 0.65a$ and $0.89a$ respectively. Right: contour plot of electrostic potential of the same equilibrium profiles

along with the scaling predicted by Porcelli from analytic theory [18]. The growth rate spectrum also

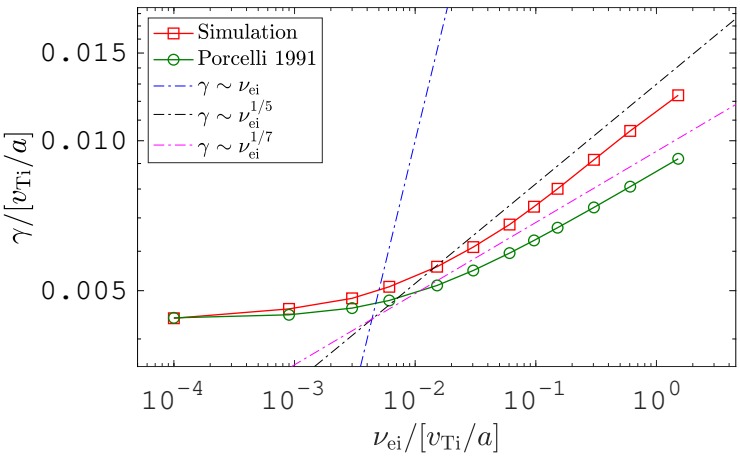


Fig. 6. Collisional Scan of $n = 1$ tearing mode using Ishizawa's profiles. The collisional scaling at low $\nu_{ei}$ (collisionless regime) is consistent with prediction by the theory by Porcelli *et al.* (1991). For the semi-collisional regime, the scaling is a bit deviated from the thoery.

shows consistent growth rates. Although the growth rates for each toroidal mode number $n$, or $k_y$, are not exactly the same because they are performed using different approaches, the comparison shows that the growth rates are consistent and within the same order of magnitude. Note that at $n = 1$, the gyrokinetic simulation can result in a larger error when performing large-scale mode simulation. [3].

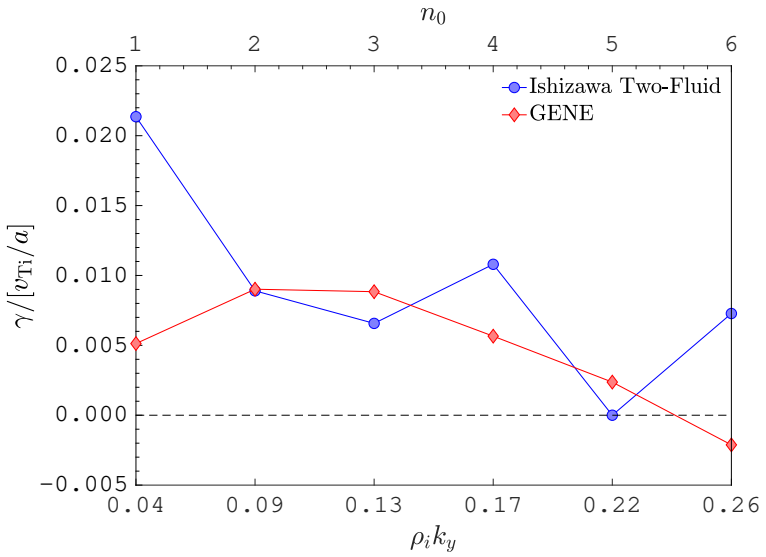


Fig. 7. Growth rate spectrum of $n = 1$ tearing mode using Ishizawa's profiles. The spectrum obtained from GENE is different from the two-fluid computation.

### *3.3. Comparison with Results of the Gyrokinetic Code GTC*

Numerical growth rates of a gyrokinetic code and reduced-MHD code can be different due to differences in computational models. For example results from gyrokinetic simulation has an inconsistency due to a large-scale-mode *ordering issue* (see [3]). Therefore a more specific comparison is performed with another gyrokinetic code. In this case GENE is compared with results from the gyrokinetic code GTC as reported in Liu *et al*. 2016 [16]. In this work, the gyrokinetic ions and finite-mass fluid electrons are used to compute standard and double tearing modes in a collisionless tokamak. For comparisons, we take the parameters and equilibrium for the case of the standard tearing mode only. The plasma parameters for the standard case are listed below.

| Simulation parameters | |
|---|---|
| Aspect ratio $(1/\varepsilon_a = R/a)$ | 10.0 |
| Electron beta $(\beta_{\rm e})$ | $4.03\times10^{-3}$ |
| Mass ratio $(m_{\rm e}/m_{\rm i})$ | 1/1836 |
| Ion gyroradius $(\rho_{\rm i}^* = \rho_{\rm i}/a)$ | $6.10\times10^{-2}$ |
| Major radius [m] | 1.68 |
| Electron skin depth $(\delta_{\rm e}/R_0)$ | $3.20\times10^{-3}$ |

The numerical $q$ profile is $q(r_a) = 1.8 + r_a^2$, where $r_a = r/a$, as shown in Fig. 8. The shifted velocity calculated using a cylindrical approximation as described in the last section is also plotted. The simulations are performed with constant pressure profiles, $T_i(r) = T_e(r) = 10$ keV and $n(r) = 0.1 \times 10^{18}$ m$^{-3}$; hence, there are no diamagnetic drift effects involved.

For the standard case with the plasma parameters listed in the table above, the numerical growth rate of the collisionless tearing mode that Liu *et al*. obtained is $\gamma_{\rm GTC} = 0.98 \times 10^{-4}\,\Omega_{\rm cp}$, where $\Omega_{\rm cp}$ is the proton cyclotron frequency. Their scan over electron skin-depth shows a growth-rate scaling that is consistent with the results derived by Drake and Lee (1977) [7], especially at small values, which has the form $\gamma_{\rm theory} = \delta_{\rm e}^2 |k'_{\parallel} v_{\rm te}| \Delta'_0 = 1.0 \times 10^{-4}\,\Omega_{\rm cp}$. A deviation is found at larger values of

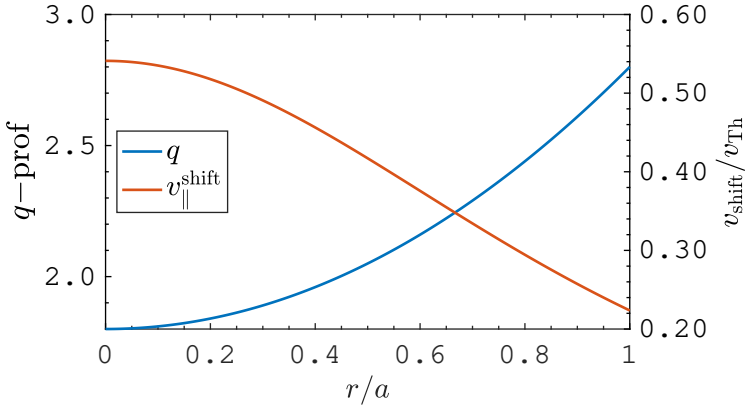


Fig. 8. The safety factor profile and the corresponding shifted velocity profile reproduced from Liu et al. (2016) [16]

$\delta_e$. Calculation by the modified GENE code with a shifted Maxwellian distribution function results in $\gamma_{\rm GENE} = 0.139\, c_{\rm ref}/L_{\rm ref} = 0.85\times 10^{-3}\,\Omega_{\rm cp}$. The result differs from that of Liu by a factor of the inverse aspect ratio. Simulation with GENE gives mode structure in the poloidal cross-section for $\phi$ and $A_{\parallel}$ that is almost identical to that of Liu. As done in Liu *et al.*, the dependence of growth rates on the electron

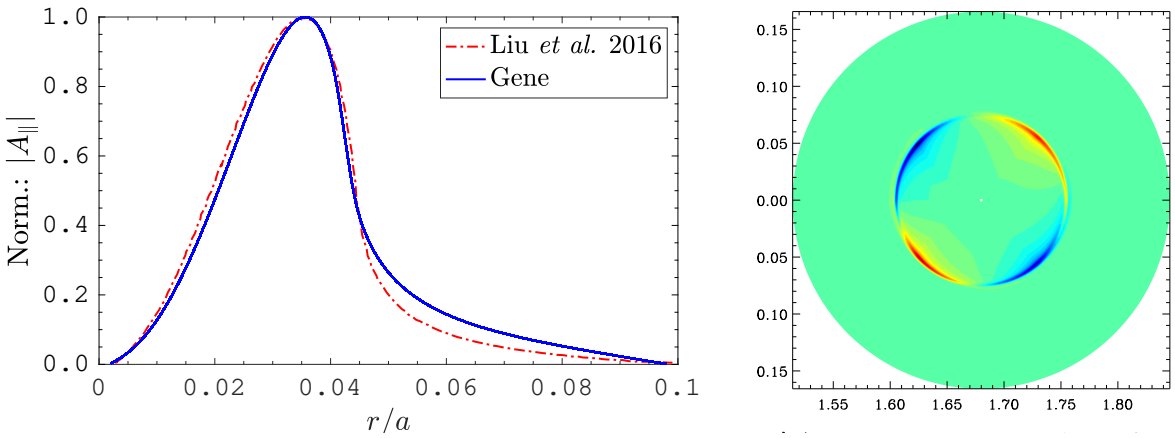


Fig. 9. [Left] Radial mode structure and [Right] the contour plot of the mode structure in poloidal-cut of the tearing mode from Liu *et al.*

skin depth is verified. In GENE, the electron skin-depth is calculated in terms of $\beta_e$; hence, the scan of electron skin-depth is equivalent to the scan of $\beta_e$

$$\delta_e = c/\omega_{pe}, \quad \text{where} \quad \omega_{pe} = \sqrt{n_{e0}e^2/\varepsilon_0 m_e}, \tag{31}$$

$$\delta_e/a = \rho_e^* \sqrt{2/\beta_e}. \tag{32}$$

The growth rate scaling with the electron skin-depth is consistent with the theory proposed in the same paper, which in turn is consistent with results predicted by Drake and Lee. This is given by

$$\gamma = \frac{k_y v_e \delta_a'}{2\sqrt{\pi} a l_s}\delta^2, \tag{33}$$

and hence, $\gamma \sim \delta_e^2 \sim 1/\beta_e$ as reproduced by GENE. We are investigating the source of the aspect

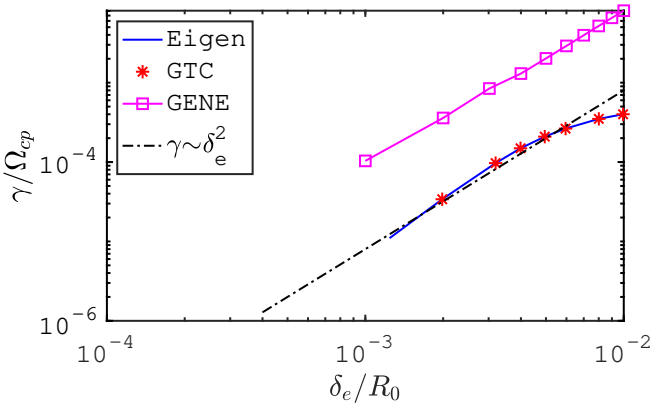


Fig. 10. Dependence of tearing mode growth rates on the electron skin-depth, or equivalently the inverted plasma beta. The growth rate scaling is as predicted by Drake&Lee (1977)

ratio factor between the growth rates calculated in the two codes. It is expected to arise from different normalizations.

### *3.4. Comparison with Results of the Gyrokinetic Code GKW*

To test the fidelity of the modified GENE code, we also have run a simulation for comparison with the published results of another gyrokinetic code, GKW. The GKW code is a $\delta f$ gyrokinetic code [17] that is modified to have shifted Maxwellian distribution functions, such that it can be used to run current-gradient-driven instabilities [12]. This test employs the equilibrium and parameters listed in the paper by Horsby et al. (2015) [13], specifically case 3 of Table 1. In this comparison temperature and density gradients are included in the simulations. The plasma beta is $\beta_e = 0.01$, $R/a = 3$, $m_e/m_i = 1/1836$, $\rho^* = \rho_i/a = \rho^*_{\text{Hornsby}}(R/a)/\sqrt{2}$. The temperature and density profiles are as shown in Fig. 11. We

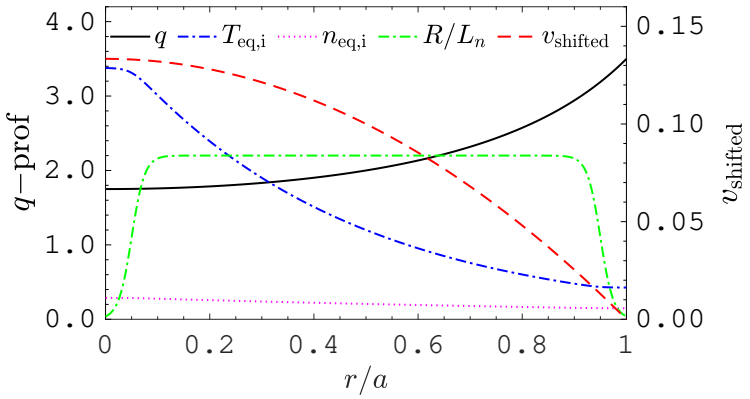


Fig. 11. Equilibrium profiles from Hornsby *et al. 2015* [13]. For $n = 1$ tearing mode, the profile exists two rational surfaces, i.e., $m = 2$ and $m = 3$.

perform the simulation with the same resolutions as stated in the paper. The mode structures obtained

from GENE are almost identical to those shown in the paper, as seen in Fig. 12. The growth rate obtained from GENE is, however, about three times larger than the published results. Here $\gamma_{\mathrm{Gene}} = 0.076\, v_{\mathrm{Th,s}}/R_0$. The discrepancy again appears to be a factor of the inverse aspect ratio ($\varepsilon_a = a/R$), which is consistent with the discrepancy found in the former comparison with Liu *et al.* Again, we expect that this discrepancy arises from different normalizations, but this needs to be verified.

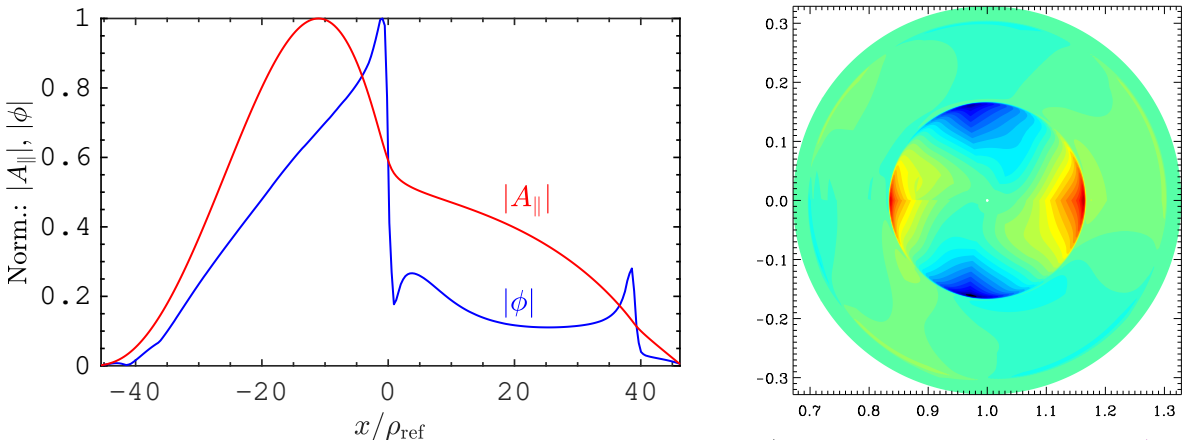


Fig. 12. Normalized radial mode structures of $A_\parallel$ and $\phi$ of the tearing mode based on Hornsby *et al.* (2016b) equilibria. The right-hand side shows the poloidal mode structure (cut at a constant toroidal angle). The structures shown the $m/n = 2/1$ mode where the first peak at $x/\rho_{\mathrm{ref}} = 0$ is corresponding to the $m = 2$, and the second peak is for $m = 3$. The $m = 2$ peak dominates.

## 4. Report Summary

Tearing-mode fluctuations are significant players in the dynamics of RFP plasmas. It has been established from simulations of nonlinear $\nabla n$-trapped electron mode turbulence with the inclusion of an external magnetic field to model tearing modes, that tearing modes suppress the zonal flow and enhance the nonlinear electrostatic flux. Further studies of the interaction of slab ITG instability with a local code utilizing a shifted Maxwellian incorporated into the perturbed distribution also indicated an effect of the tearing modes on the ITG turbulence level. However these studies did not realistically model self-consistent global tearing modes. They lacked curvature effects and terms that are important in three-dimensional geometries. The slab study also exhibited an intermediate-scale instability of unknown identity that interfered with analysis of the multiscale interaction between the tearing and ITG modes. Consequently, work described in this report was undertaken to modify the gyrokinetic code GENE to include current-gradient-drive terms arising from a shifted Maxwellian in the equilibrium distribution function. Implementation of the shifted Maxwellian distribution in the governing gyrokinetic equations of GENE enables realistic calculations of toroidal tearing mode instability and its nonlinear evolution self-consistently. The implementation includes modifying higher velocity moments to obtain physical observables under the shifted Maxwellian.

We tested the modified code and corresponding computational routines against other computational tools in different regimes. A comparison first was performed against a local flux-tube simulation, which is well-established in the study of microtearing physics. The simulation results from the two codes show consistent growth rates at low plasma beta ($\beta_{\mathrm{e}}$). At higher beta, the codes reveal deviations,

especially at lower mass ratios. The global simulations, however, show the scaling of $1/\sqrt{\beta}$ in the growth rates, consistent with theoretical predictions. When the equilibria from the fluid simulation of Ishizawa *et al.* were introduced for further testing, the modified GENE code produced mode structures that are nearly identical with the mode structures of the fluid calculation. The collisional scan and growth rate spectrum display characteristic behavior of global tearing modes. This establishes that the modified GENE code captures global tearing-mode dynamical behavior. The code was also tested against the discrete gyrokinetic PIC code GTC. The original work performed by Liu *et al.* utilized gyrokinetic ions and fluid electrons for simplicity. The mode structures obtained from these different codes are almost identical. The scan over electron skin-depth shows consistent results, especially in terms of the scaling known from theory. However, the growth rates are different by a factor of the aspect ratio. The same discrepancy is observed in the simulation using the equilibrium from Hornsby *et al.*, which performs the linear tearing mode calculation using a continuous gyrokinetic code, GKW. The growth rate obtained from GENE differs from the GKW code by a factor of the aspect ratio. However, the two codes have the same mode structures.

It has thus been shown that the modified Gene code allows us to reproduce linear global tearing modes under different plasma equilibria. It is shown that the code yields radial and toroidal mode structures, as well as the correct scalings under scans over plasma parameters. The signatures of the tearing modes as predicted by established theories are also recovered. The discrepancy believed to arise from an aspect-ratio factor in normalizations remains to be fully resolved.

## References


1. D. Carmody, M. Pueschel, J. Anderson, and P. Terry. Microturbulence studies of pulsed poloidal current drive discharges in the reversed field pinch. *Physics of Plasmas*, 22(1):012504, 2015.
2. B. Chapman, J. Ahn, A. Almagri, J. Anderson, F. Bonomo, D. Brower, D. Burke, K. Caspary, D. Clayton, S. Combs, et al. Improved-confinement plasmas at high temperature and high beta in the mst rfp. *Nuclear fusion*, 49(10):104020, 2009.
3. J. P. M. Collar, B. F. McMillan, S. Saarelma, and A. Bottino. Comparing electromagnetic instabilities in global gyrokinetic simulations with local and mhd models. *Plasma Physics and Controlled Fusion*, 62(9):095005, 2020.
4. A. Di Siena. *Implementation and investigation of the impact of different background distributions in gyrokinetic plasma turbulence studies*. 2019.
5. A. Di Siena, A. Biancalani, T. Görler, H. Doerk, I. Novikau, P. Lauber, A. Bottino, and E. P. and. Effect of elongation on energetic particle-induced geodesic acoustic mode. *Nuclear Fusion*, 58(10):106014, aug 2018.
6. A. Di Siena, T. Görler, H. Doerk, R. Bilato, J. Citrin, T. Johnson, M. Schneider, E. Poli, and J. Contributors. Non-maxwellian fast particle effects in gyrokinetic gene simulations. *Physics of Plasmas*, 25(4):042304, 2018.
7. J. Drake and Y. Lee. Kinetic theory of tearing instabilities. *The Physics of Fluids*, 20(8):1341–1353, 1977.
8. F. Ebrahimi, V. Mirnov, S. Prager, and C. Sovinec. Momentum transport from current-driven reconnection in the reversed field pinch. *Physical review letters*, 99(7):075003, 2007.
9. G. Fiksel, S. Prager, W. Shen, and M. Stoneking. Measurement of magnetic fluctuation induced energy transport. *Physical review letters*, 72(7):1028, 1994.
10. Y. Ho and G. Craddock. Nonlinear dynamics of field maintenance and quasiperiodic relaxation in reversed-field pinches. *Physics of Fluids B: Plasma Physics*, 3(3):721–734, 1991.
11. S. Hokin, A. Almagri, S. Assadi, J. Beckstead, G. Chartas, N. Crocker, M. Cudzinovic, D. Den Hartog, R. Dexter, D. Holly, et al. Global confinement and discrete dynamo activity in the mst reversed-field pinch. *Physics of Fluids B: Plasma Physics*, 3(8):2241–2246, 1991.
12. W. Hornsby, P. Migliano, R. Buchholz, L. Kroenert, A. Weikl, A. Peeters, D. Zarzoso, E. Poli, and F. Casson. The linear tearing instability in three dimensional, toroidal gyro-kinetic simulations. *Physics of Plasmas*, 22(2):022118, 2015.
13. W. A. Hornsby, P. Migliano, R. Buchholz, S. Grosshauser, A. Weikl, D. Zarzoso, F. J. Casson, E. Poli, and A. G. Peeters. The non-linear evolution of the tearing mode in electromagnetic turbulence using gyrokinetic simulations. *Plasma Physics and Controlled Fusion*, 58(1):014028, 2015.
14. A. Ishizawa, Y. Kishimoto, and Y. Nakamura. Multi-scale interactions between turbulence and magnetic islands and parity mixture—a review. *Plasma Physics and Controlled Fusion*, 61(5):054006, 2019.
15. A. Ishizawa and N. Nakajima. Thermal transport due to turbulence including magnetic fluctuation in externally heated plasma. *Nuclear fusion*, 49(5):055015, 2009.
16. D. Liu, J. Bao, T. Han, J. Wang, and Z. Lin. Verification of gyrokinetic particle simulation of current-driven instability in fusion plasmas. iii. collisionless tearing mode. *Physics of Plasmas*, 23(2):022502, 2016.
17. A. Peeters, Y. Camenen, F. J. Casson, W. Hornsby, A. Snodin, D. Strintzi, and G. Szepesi. The nonlinear gyro-kinetic flux tube code gkw. *Computer physics communications*, 180(12):2650–2672, 2009.
18. F. Porcelli. Collisionless m= 1 tearing mode. *Physical review letters*, 66(4):425, 1991.
19. M. J. Pueschel, F. Jenko, D. Told, and J. Büchner. Gyrokinetic simulations of magnetic reconnection. *Physics of Plasmas*, 18(11):112102, 2011.
20. Z. Williams. *On the Interactions of Magnetic Fluctuations, Zonal Flows, & Microturbulence in Fusion Plasmas*. 2019.
21. Z. Williams, M. Pueschel, P. Terry, and T. Hauff. Turbulence, transport, and zonal flows in the madison symmetric torus reversed-field pinch. *Physics of Plasmas*, 24(12):122309, 2017.